Received 27 June 2023; accepted 7 August 2023. Date of publication 3 October 2023;
date of current version 22 November 2023. The review of this article was arranged by Associate Editor M. Toda.

Digital Object Identifier 10.1109/OJNANO.2023.3318236

Design, Fabrication and Measurement of Radio Frequency Micro-Electro-Mechanical Systems

GIRIJA SRAVANI KONDAVITEE [1] (Member, IEEE), YOUNG SUH SONG [2,3] (Member, IEEE), SRINIVASA RAO KARUMURI [1] (Member, IEEE), KOUSHIK GUHA [4] (Member, IEEE), BRAJESH KUMAR KAUSHIK [5] (Senior Member, IEEE), AND AIMÉ LAY-EKUAKILLE [6] (Senior Member, IEEE)

[1]MEMS Research Center, Department of ECE, Koneru Lakshmaiah Educational Foundation (Deemed to be University), Guntur, AP 522502, India
[2]Inter-University Semiconductor Research Center, Department of Electrical and Computer Engineering, Seoul National University, Seoul 08826, South Korea
[3]Department of Computer Science, Korea Military Academy, Seoul 01805, South Korea
[4]Department of Electronics and Communication Engineering, National Institute of Technology, Silchar, Assam 788010, India
[5]Department of Electronics and Communication Engineering, Indian Institute of Technology, Roorkee 600036, India
[6]Department of Innovation Engineering, University of Salento, 73100 Lecce, Italy

CORRESPONDING AUTHOR: GIRIJA SRAVANI KONDAVITEE. (e-mail: kondavitee.sravani03@gmail.com)

ABSTRACT This article describes the fabrication and experimental results of a novel step structure Radio Frequency Microelectromechanical system (RF MEMS) switch integrated with a circular patch antenna. The RF MEMS switch is developed using surface micromachining technology and exhibits several desirable characteristics. The key findings and features of the proposed RF MEMS switch are as follows: The switch operates at a very low pull-in voltage of 4.4 V, which is advantageous as it requires low actuation voltage for switching operations. Low ON State Capacitance: The switch demonstrates a low ON state capacitance of 81.2 fF, indicating efficient switching performance. High Isolation: The switch exhibits high isolation of −60.68 dB at 23 GHz, which is the central frequency of the K-band. This high isolation ensures minimal interference and improved signal integrity. The RF MEMS switch is integrated with a circular patch antenna, enabling reconfigurability in the operating frequency of the antenna. The antenna's frequency can be adjusted by actuating the switches alternatively. The specific operating frequencies and return loss values are as follows: Both Switches ON: The antenna radiates the signal at a frequency of 19.2 GHz with a return loss of −26.7 dB. Only Switch A ON: The antenna radiates at a frequency of 21 GHz with a return loss of −17.6 dB. Only Switch B ON: The antenna radiates the signal at a frequency of 26.4 GHz with a return loss of −17.47 dB. The RF MEMS switch and antenna are optimized to transmit RF signals within the K-band frequency range. The integration of the step structured RF MEMS switches successfully enables reconfiguration of the antenna's operating frequency. The proposed antenna, integrated with the RF MEMS switches, has potential applications in various K-band systems, including surface movement radars, direct broadcast satellite, Direct-to-Home (DHT) television, and 5th Generation (5G) mobile communication. The reconfigurability of the antenna's frequency allows for flexibility and adaptability in different K-band applications.

INDEX TERMS RF MEMS switch, pull-in voltage, return loss, insertion loss, isolation, surface micromachining, antenna, reconfigurability.

I. INTRODUCTION

Micromachining plays a crucial role in the development of low-power and low-cost miniaturized RF MEMS switches. Extensive research has been conducted by academics, research laboratories, and companies in this field. RF MEMS switches are classified into different types, including series or shunt switches, cantilever or bridge-type switches, and metal-to-metal contact or capacitive switches. The main driving force behind the development of RF MEMS switches is their high RF performance in frequencies above 10 GHz.

© 2023 The Authors. This work is licensed under a Creative Commons Attribution 4.0 License. For more information, see https://creativecommons.org/licenses/by/4.0/

Compared to semiconductor switches such as PIN diodes, FETs, and variable capacitors, RF MEMS switches operate at low DC power levels, typically in the range of microwatts. This focus on RF MEMS switches is driven by the need for high-performance switches in the frequency range above 10 GHz, as well as the advantage of low power consumption compared to semiconductor switches. The use of micromachining techniques enables the fabrication of miniaturized switches with enhanced RF performance and lower power requirements.

The reliability of RF MEMS switches is a critical concern and can be affected by several factors. Surface roughness of the dielectric layers plays a significant role in the switch's operating frequency. Increased surface roughness reduces the contact area between the membrane and the dielectric, resulting in decreased downstate capacitance and ultimately affecting the RF performance of the switch. Stiction is another reliability issue that occurs during the release process when liquid residues from cleaning solutions, such as Isopropyl alcohol (IPA) and acetone, remain on the surface of the dielectric layer, causing sticking problems. The lifetime of the switches is limited without the implementation of a proper compliant mechanism. The low spring constant offered by meandered hinges makes the membrane susceptible to buckling and reduces its ability to hold its position effectively. To develop more reliable RF MEMS switches, it is essential to optimize the design and address these challenges. The capacitance ratio of the switch, often referred to as the Figure of Merit, indicates the efficiency of the switch in transmitting high-frequency RF signals. One way to improve the Figure of Merit is by reducing the insertion loss of the switch. Increasing the upstate capacitance is a primary method to achieve this. Previous research has focused on reducing upstate capacitance through material selection and optimizing beam dimensions. However, frequent material changes can negatively impact the switch's robustness, and large suspended beams can increase insertion loss and transition time.

The main objective of the article is to design and develop a novel step-structured RF MEMS switch specifically for K-band applications using surface micromachining technology. The key significance of the novel step structure is to reduce the pull-in voltage by incorporating two different variable air gaps between the electrodes and the beam. This unique switch structure aims to achieve low insertion loss and high isolation during RF signal propagation. It should be noted that, until now, no switch with a step-structured beam has been fabricated, making this article's contribution novel. The article provides a detailed step-by-step procedure of the fabrication process, which is primarily carried out in a clean room environment with class 100 and class 1000 cleanliness standards.

The structure of the article is organized as follows: Section II: Proposed Device and Dimensions In this section, the article presents the proposed device, which is the step-structured RF MEMS switch, along with its dimensions. The design considerations and specifications of the device are discussed, highlighting its relevance to K-band applications. Section III: Fabrication Steps This section focuses on explaining the fabrication steps involved in manufacturing the proposed step-structured switch. It provides a detailed description of the surface micromachining technology utilized and the specific processes employed to create the switch's structure. The clean room procedures, materials used, and key fabrication techniques are outlined. Section IV: Electrical, Mechanical, and Electromagnetic Characteristics In Section IV, the electrical, mechanical, and electromagnetic characteristics of the step-structured switch are thoroughly investigated. The switch is subjected to various tests and characterizations using different measurement techniques. DC measurements are performed to analyze the electrical behavior, while LDV (Laser Doppler Vibrometer) measurements are used to evaluate the mechanical response. RF probe stations are employed to assess the switch's electromagnetic performance, including parameters such as insertion loss, isolation, and frequency reconfigurability. Section V: Conclusive Considerations and Future Outlook The article concludes with Section V, which summarizes the main findings and conclusions drawn from the study. It highlights the significance of the proposed step-structured switch in terms of its low insertion loss, high isolation, and suitability for K-band applications. Additionally, this section outlines future directions and potential areas for further exploration and development in the field of RF MEMS switches.

II. THE PROPOSED DEVICE AND ITS DIMENSIONS

The RF MEMS switch described in the article follows a general structure that includes the following components:

1) *Substrate:* The switch is built on a substrate material, providing a foundation for the device.
2) *Insulating Layer:* An insulating layer is deposited on the substrate to electrically isolate the switch components.
3) *Signal Line:* The switch incorporates a signal line in the form of a coplanar waveguide (CPW). The CPW carries the RF signal through the switch.
4) *Beam and Anchors:* In shunt switches, a beam is supported by anchors at both ends. The beam is movable and can be actuated to switch between ON and OFF states.
5) *Capacitive Configuration:* In the capacitive configuration, the switch allows the signal to pass between the input and output terminals when the beam is in the upstate (ON state). When a pull-in voltage is applied, the beam is pulled down, turning off the switch and preventing the RF signal from passing through. This is the OFF state of the capacitive shunt switch.
6) *Step-Structured Beam:* The proposed switch incorporates a step-structured beam design. This design feature aims to reduce insertion and return losses, improving the switch's overall performance.
7) *Non-Uniform Structured Meanders:* The beam is suspended by non-uniform structured meanders. This

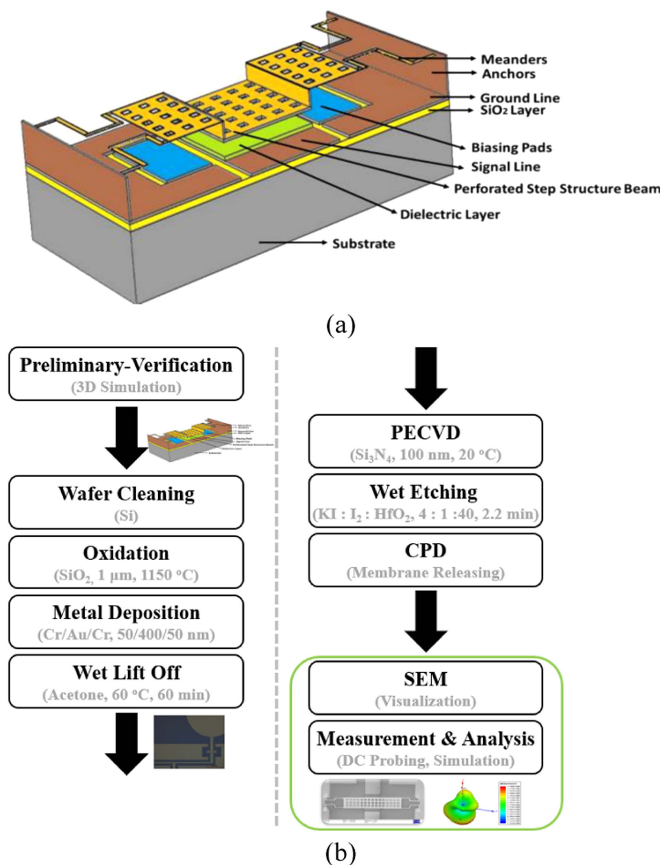

FIGURE 1. (a) Three-dimensional (3D) view of step structured switch, and (b) overall workflow of this research.

TABLE 1. Proposed Device Specifications

Component	Optimized Dimensions (l×b×h in µm)	Material
Substrate	540×600×840	Silicon
Insulating layer	540×600×2	Silicon dioxide
Signal line	120×600×1	Gold
Dielectric layer	120×150×0.1	Silicon nitride
Biasing Pads	80×140×1.1	Gold
Ground Planes	140×600×1	Gold
Central Beam	120×140×0.5	Gold
Side Beams	100×140×0.5	Gold
gap b/w Signal Line and Ground Planes	70	---
Air gap b/w central beam and dielectric	2	Air
Air gap b/w side beams and biasing pads	4	Air

FIGURE 2. Silicon wafers, (a) cleaned wafers (b) single side polished wafers.

design choice helps to lower the pull-in voltage required to actuate the switch.

The top view of the proposed switch structure is illustrated in Fig. 1(a), and the dimensions of the components are provided in Table 1. Fig. 1(b) depicts the overall workflow of the research, indicating the progression of the study from design to fabrication and characterization. By incorporating the step-structured beam and non-uniform structured meanders, the proposed RF MEMS switch aims to enhance its performance in terms of insertion loss, return loss, and pull-in voltage requirements.

III. FABRICATION

A. WAFER PROCESSING

In the fabrication process of the proposed step structure RF MEMS switch, surface micromachining is employed. The first step in this process is wafer processing, which involves the following steps:

1) *Wafer Selection:* A single-side polished P-type 4-inch silicon wafer with the '100' orientation is chosen as the substrate. The wafer has a thickness of 500 µm and a resistivity of approximately 10 Ω/m [20].
2) *Cleaning:* To remove metal and organic contaminants from the wafer, a cleaning process is performed. In this fabrication process, the RCA (Radio Corporation of America) cleaning method is utilized. The RCA process involves a series of cleaning steps using a combination of chemicals and deionized water to achieve thorough wafer cleaning (Fig. 2).

It's important to note that the specific details and parameters of the RCA cleaning process may vary depending on the requirements of the fabrication facility and the desired level of cleanliness.

B. THERMAL OXIDATION

In order to isolate the coplanar waveguide (CPW) from the silicon substrate, a layer of silicon dioxide (SiO2) is grown on the substrate using the thermal oxidation method. The thermal oxidation process involves subjecting the wafer to high temperatures in an oxygen-rich environment. In this case, the wafer is heated to 1150 °C, causing the silicon atoms on the wafer surface to react with oxygen and form a layer of silicon dioxide. The thermal oxidation process results in the growth of a SiO2 layer with a thickness of up to 1 µm on the substrate. This SiO2 layer acts as an insulating layer, providing electrical isolation between the CPW waveguide and the silicon substrate. By preventing leakage currents and unwanted electrical coupling with the substrate, the SiO2 layer helps to reduce

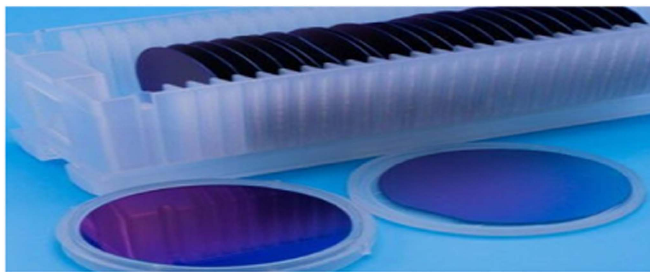

FIGURE 3. Oxidised silicon wafers.

FIGURE 4. Patterned wafers (a) proposed switch region (b) antenna circular patch region.

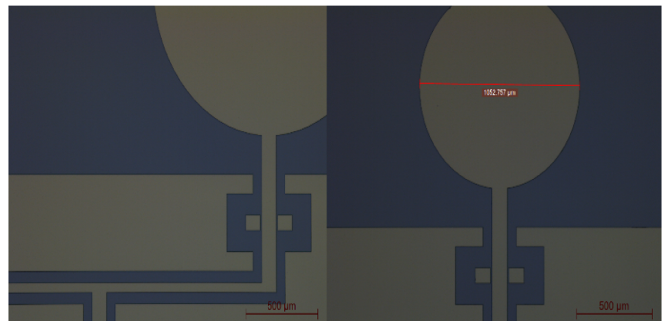

FIGURE 5. Metal deposition on the specified region (a) proposed switch region (b) antenna circular patch region.

losses in the signal transmission through the waveguides. The thermal oxidized wafers exhibit a blue coloration on the top surface, which can be seen in Fig. 3 of the article. This blue color is a visual indication of the presence of the SiO2 layer on the substrate.

C. DEPOSITION OF METAL FOR ANTENNA, CPW AND BIASING PADS

To define the CPW feed, antenna patches, and biasing pads in the proposed structure, a lithography process is employed Fig. 4. Lithography is a widely used technique in microfabrication that allows for precise patterning of structures on a substrate.

The lithography process involves the following steps:

1) *Photoresist (PR) coating:* A layer of photoresist material is applied to the surface of the substrate, which in this case is the SiO2 layer on the silicon substrate. The photoresist acts as a light-sensitive material that undergoes chemical changes upon exposure to specific wavelengths of light.
2) *Mask alignment and exposure:* A mask, which contains the desired pattern of the CPW feed, antenna patches, and biasing pads, is aligned with the coated substrate. The mask has transparent regions that allow light to pass through and expose the underlying photoresist. The alignment ensures proper positioning of the pattern on the substrate.
3) *UV exposure:* The aligned substrate and mask are exposed to ultraviolet (UV) light, which passes through the transparent regions of the mask and reaches the photoresist-coated substrate. The UV light causes chemical reactions in the exposed areas of the photoresist, resulting in changes in its solubility or cross-linking properties.
4) *Development:* After UV exposure, the substrate is subjected to a development process, which typically involves immersing it in a developer solution. The developer selectively removes either the exposed or unexposed areas of the photoresist, depending on the type of photoresist used (positive or negative resist). This step reveals the desired pattern on the substrate.
5) *Etching or deposition:* Depending on the specific requirements of the CPW feed, antenna patches, and biasing pads, subsequent steps such as etching or deposition may be performed. Etching is used to remove material selectively from the substrate or the deposited metal, while deposition adds a layer of material onto the substrate surface Fig. 5.

By using lithography, the desired shapes and dimensions of the CPW feed, antenna patches, and biasing pads are precisely defined on the substrate, allowing for efficient propagation of RF signals within the desired frequency range.

To ensure good adhesion between the gold (Au) and the SiO2 layer, a Cr/Au/Cr stack is utilized for defining the CPW transmission line, antenna patches, and biasing pads. The stack consists of a layer of chromium (Cr) sandwiched between two layers of gold. The deposition of the Cr/Au/Cr stack is carried out using the DC sputtering physical vapor deposition (PVD) process. DC sputtering deposition is chosen for its higher deposition rate compared to RF sputtering, making it more efficient for this application. The specific thickness of the layers in the stack is as follows: Cr [50 nm] / Au [400 nm] / Cr [50 nm]. The deposition process is performed at a distance of 7.5 cm on a 4-inch wafer for a duration of 3 hours. After the metal deposition, a wet lift-off process is employed to remove the unwanted metal and retain the desired pattern. The wafer is placed in a PG remover solution, typically consisting of acetone, and subjected to a temperature of 60 °C for approximately 60 minutes. During this time, the metal that was deposited over the photoresist (PR) layer will be lifted off. Once the lift-off process is complete, the remaining Cr/Au/Cr stack, which is present over the SiO2 layer, will

remain intact, defining the CPW transmission line, antenna patches, and biasing pads. Finally, the wafer is cleaned with deionized (DI) water to remove any residual contaminants or chemicals. This ensures the substrate is ready for further processing and characterization. The result of this process is the formation of the desired metal structures on the substrate, which play a crucial role in transmitting and manipulating RF signals in the proposed RF MEMS switch.

D. DIELECTRIC LAYER DEPOSITION

During the fabrication of the proposed capacitive step structured RF MEMS switch, the choice of dielectric material and its relative permittivity greatly influences the RF transmission properties. In this case, silicon nitride (Si3N4) is selected as the dielectric material due to its high relative permittivity of 7.5. To ensure the dielectric layer is present only over the signal line at the specified region and dimensions, a patterning process is carried out using lithography. A photoresist (PR) material is coated over the entire wafer, including the silicon nitride layer. Through lithography, a portion of the PR is retained in the areas where the silicon nitride should remain, while the rest of the PR is removed. This defines the pattern for the subsequent etching process. Reactive Ion Etching (RIE) is employed as a dry etch process to remove the unprotected silicon nitride layer. In this step, the wafer is placed in an RIE-Cl equipment, where the unprotected silicon nitride layer reacts with chlorine (Cl) gases. The RIE process is carried out for a duration of 6 minutes. At the end of the etching process, an ashing step is performed to ensure better removal of residues. Ashing involves subjecting the wafer to a suitable treatment, such as plasma ashing, to eliminate any remaining organic or inorganic contaminants. The specific specifications of the equipment used during the RIE-Cl process may vary depending on the setup and equipment employed. It is important to follow the recommended parameters and conditions provided by the equipment manufacturer or established process guidelines to achieve the desired results. Overall, this process enables the precise patterning of the silicon nitride dielectric layer, ensuring it is selectively present only in the desired areas of the RF MEMS switch structure.

- *Power:* ICP- 1800 /RF-200
- *Gas Flow:* 24
- *Temperature:* 20 ^{o}C
- *Chamber Pressure:* 2mT
- *Helium (T):* 10
- *Time Taken:* 1.47

In the fabrication process of the proposed capacitive step structured RF MEMS switch, the silicon nitride layer is selectively patterned on the signal line of the coplanar waveguide (CPW) at the specified region and dimensions. Initially, after the lithography process, the photoresist (PR) material is present over the entire wafer, including the silicon nitride layer, as shown in Fig. 6(a).

Following the lithography step, the wafer undergoes Reactive Ion Etching (RIE) using chlorine (Cl) gases to remove the unprotected silicon nitride layer. After the RIE process, ashing is performed to ensure the complete removal of any residues. As a result, the silicon nitride layer remains only in the specified region where it was protected by the PR, as illustrated in Fig. 6(b).

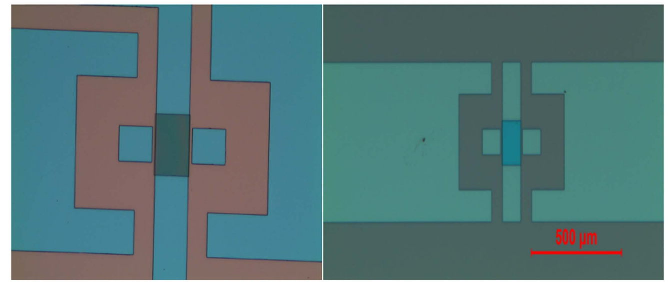

FIGURE 6. Dielectric layer deposition on the specified region (a) silicon nitride layer protected with PR (b) portion of the switch after ashing.

The presence of the PR material in Fig. 6(a) indicates the areas where the silicon nitride layer is desired, while the absence of the PR material in Fig. 6(b) signifies the successful patterning and retention of the silicon nitride layer only in the intended regions of the CPW signal line.

This selective deposition of the silicon nitride dielectric layer ensures that the RF signal propagation occurs through the designated areas, maintaining the desired transmission properties of the RF MEMS switch.

E. DEPOSITION OF MEMBRANE AND ANCHORS

To achieve the desired suspended membrane structure with a 2 µm air gap between the silicon nitride layer and the membrane, additional fabrication steps are required in the process of developing the capacitive step structured RF MEMS switch. After the silicon nitride patterning step, a sacrificial layer is typically deposited over the entire wafer to create the required air gap. The sacrificial layer acts as a support during the fabrication process and is later removed to create the suspended structure. Common sacrificial materials include polymers such as SU-8 or sacrificial oxide layers. Once the sacrificial layer is deposited, a protective layer or mask can be applied to define the region where the membrane will be suspended. This protective layer ensures that the sacrificial layer is only removed in the specified area, allowing for the formation of the air gap. Next, a selective etching process, such as a wet or dry etching method, is employed to remove the sacrificial layer from the designated region, leaving the desired air gap between the silicon nitride layer and the membrane. The etching process is carefully controlled to ensure the membrane remains intact and suspended over the CPW transmission line. After the successful formation of the suspended membrane structure with the specified air gap, further steps can be carried out to characterize and test the RF properties of the fabricated RF MEMS switch. It is important to note that the exact fabrication process steps and parameters may vary depending on the specific fabrication techniques and equipment used in the clean room facility. The process described

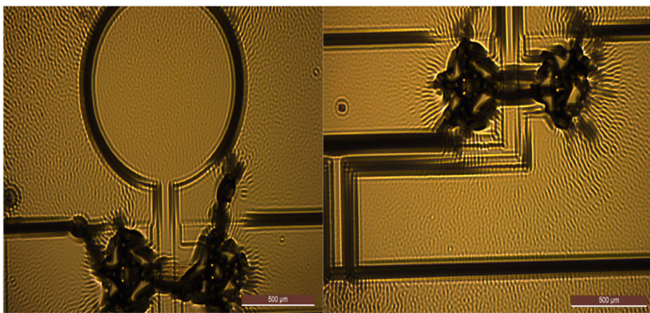

FIGURE 7. Metal deposition on wafer (a) antenna patch region (b) proposed switch region.

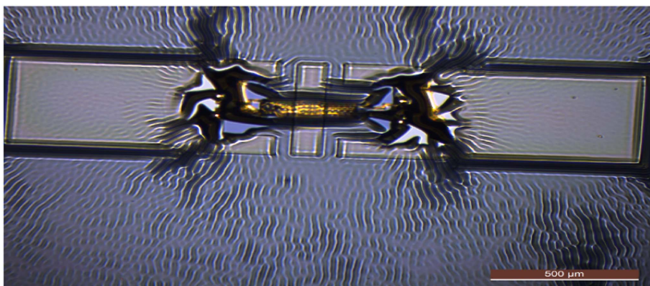

FIGURE 8. Membrane and anchor region after etching.

here provides a general overview of the steps involved in achieving the desired membrane suspension with an air gap of 2 μm over the CPW transmission line Fig. 7.

In the fabrication process of the capacitive step structured RF MEMS switch, wet etching is employed to pattern the membrane metal layer (Au) in the specified region. The wet etching process involves the use of a developer solution consisting of KI:I2:H2O in a ratio of 4:1:40. The developer solution is responsible for selectively etching away the unwanted portion of the deposited metal layer.

Here are the details of the wet etching process:

- *Developer Solution:* KI:I2:H2O in a ratio of 4:1:40
- *Etching Rate:* 240 nm/second (This rate indicates the amount of metal etched per unit time)
- *Developing Time:* 2.2 minutes (The duration for which the wafer is immersed in the developer solution)
- *Temperature:* Room temperature (Typically around 25 degrees Celsius)

During the wet etching process, the developer solution selectively reacts with the exposed metal layer, removing the undesired portions while leaving the protected regions intact. This results in the patterned membrane metal layer, as shown in Fig. 8. It is important to carefully control the etching parameters, such as the etching rate, developing time, and temperature, to ensure precise patterning of the membrane metal layer without affecting the underlying layers or structures

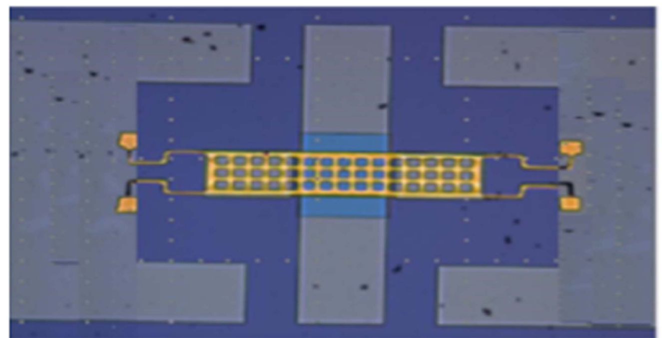

FIGURE 9. Membrane released after CPD.

F. RELEASING PROCESS

Releasing the MEMS structure, such as the membrane, is indeed a critical step in MEMS device fabrication. The release process involves removing sacrificial or supporting layers to free the suspended structures and enable their functionality. Chemical processes are commonly used for releasing MEMS structures, and various methods can be employed depending on the specific design and materials involved. One commonly used technique for releasing MEMS structures is wet etching. In this process, a selective etchant is used to dissolve the sacrificial material while leaving the desired structures intact. The etchant chosen depends on the sacrificial material used. For example, if a sacrificial layer of silicon dioxide (SiO2) is used, hydrofluoric acid (HF) can be employed as an etchant to dissolve the SiO2 layer selectively.

The releasing process typically involves the following steps:

1) *Protecting the desired structures:* Prior to etching, any structures that need to be protected from the etchant are usually coated or covered with a protective layer, such as a photoresist or another suitable masking material.
2) *Applying the etchant:* The etchant is applied to the wafer or substrate, either by immersion or by spin-coating, depending on the specific requirements. The etchant selectively dissolves the sacrificial layer while leaving the protected structures unaffected.
3) *Monitoring and controlling the etching process:* The etching process is carefully monitored to ensure the sacrificial layer is fully removed while avoiding over-etching or damage to the desired structures. Etching time, temperature, and other parameters are controlled to achieve the desired release.
4) *Rinse and clean:* After the sacrificial layer is completely removed, the wafer is thoroughly rinsed with suitable solvents or deionized water to remove any residues from the etching process Fig. 9.

In Fig. 10, the SEM image would likely showcase the detailed morphology and structural features of the fabricated RF MEMS switch. The image would have a high magnification, allowing for a close examination of the switch's components, such as the suspended membrane, the CPW transmission line,

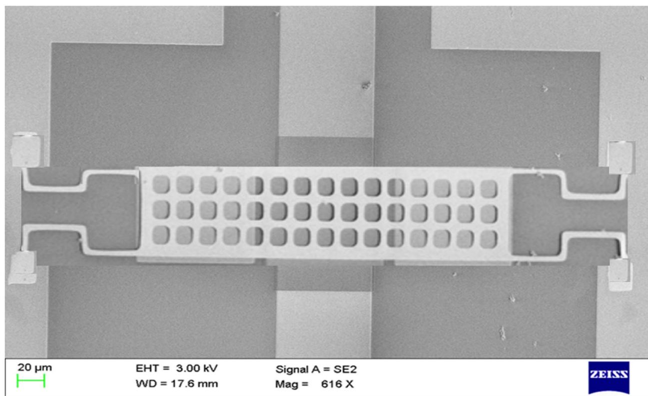

FIGURE 10. SEM image of fabricated switch.

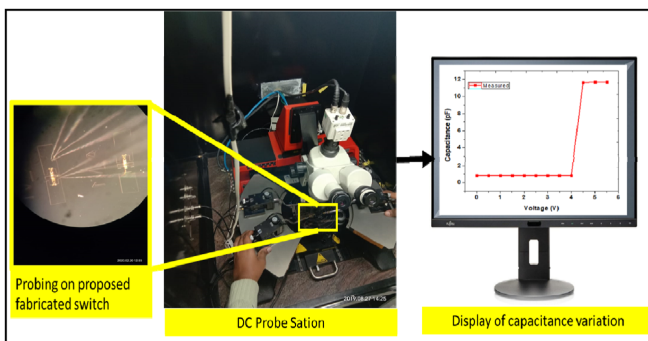

FIGURE 11. DC probing on proposed fabricated switch.

and the surrounding structures. The SEM image would reveal the surface topography of the switch, providing information about the dimensions, shapes, and alignment of the different elements. It can help assess the quality of the fabrication process, including the patterning, deposition, and etching steps. Additionally, the SEM image can highlight the interfaces between different materials, such as the adhesion of the metal layers to the dielectric or substrate. By analyzing the SEM image, researchers can evaluate the uniformity, integrity, and precision of the fabricated switch. They can also identify any potential defects, such as surface roughness, debris, or unintended variations in the dimensions or shapes of the components.

IV. CHARACTERIZATIONS

The proposed RF MEMS switch with integrated circular patch antennas has undergone thorough characterization to evaluate its electrical, mechanical, and electromagnetic performance. The characterization process involved measuring various parameters using specialized equipment. For the electrical characterization, the DC Probe station in the Micro and Nano Characterization Facility (MNCF) bay was used Fig. 11. The Pull-in voltage, Upstate capacitance, and Downstate capacitance were measured to assess the electrical behavior of the switch. These measurements provide important insights into the actuation voltage required to switch the device, as well as the capacitance values in different states of the switch. The mechanical resonant frequency of the switch was determined using a Microsystem Analyzer (MSA). This measurement helps to identify the natural resonant frequency of the switch structure, which is crucial for its mechanical stability and performance. The electromagnetic characterization of the switch was performed using an RF probe station, also known as a Vector Network Analyzer (VNA). The VNA allows for the measurement of key electromagnetic parameters, including return loss (S11), insertion loss (S12), and isolation loss (S21). These measurements provide insights into the switch's ability to transmit and receive RF signals efficiently, as well as its isolation characteristics. By conducting these comprehensive measurements, researchers can assess the overall performance and functionality of the fabricated RF MEMS switch. The characterization results enable a thorough understanding of its electrical, mechanical, and electromagnetic properties, which are essential for its successful integration and application in RF systems.

A. ELECTRICAL CHARACTERISTICS

In the measurement setup using the DC probe station, the fabricated RF MEMS switch with integrated antennas is carefully loaded onto the station. The biasing pads of the switch are connected to a DC voltage source, while the ground terminal is connected to the ground lines of the coplanar waveguide (CPW). By applying a DC voltage to the biasing pads, an electrostatic force is generated within the switch structure. Since the switch membrane is connected to the ground terminals, this electrostatic force acts on the membrane, causing it to move or deform. This movement or deformation of the membrane is essential for the operation of the RF MEMS switch. By controlling the applied DC voltage, the researchers can observe the behavior of the switch, including the pull-in voltage, upstate capacitance, and downstate capacitance. These measurements provide valuable information about the electrical characteristics and performance of the switch. The DC probe station provides a controlled environment for conducting these electrical measurements, ensuring accurate and reliable data acquisition. This setup allows researchers to analyze the response of the switch under different voltage conditions and evaluate its suitability for RF applications.

To characterize the displacement of the switch beam during actuation and deactivation, a range of DC voltages is applied to the biasing pads. The voltage is varied from 0 V to 6 V for actuation, causing the membrane to move and change its position. Similarly, negative voltages from −6 V to 0 V are applied to deactivate the membrane and return it to its original position Fig. 12. During this process, the displacement of the switch beam is carefully measured and recorded. The displacement values at different applied voltages provide insights into the behavior and performance of the RF MEMS switch. These measurements help determine the response of

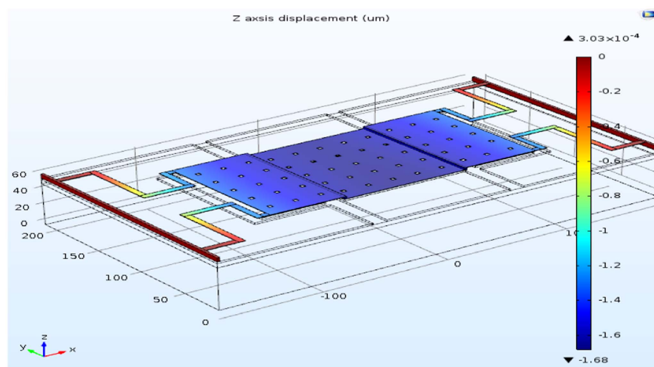

FIGURE 12. Simulation of proposed switch for displacement.

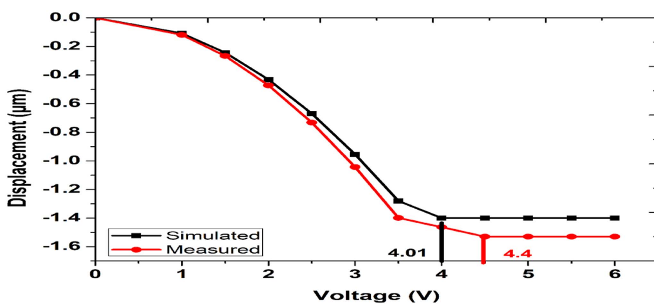

FIGURE 13. Displacement analysis of proposed switch (simulated & measured).

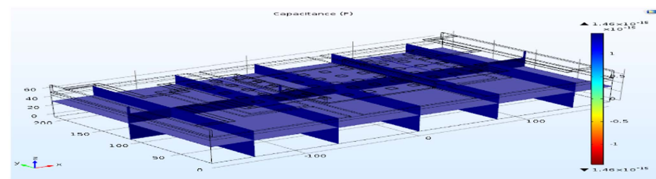

FIGURE 14. Upstate capacitance simulated using FEM tool.

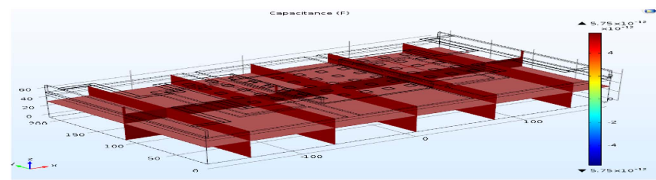

FIGURE 15. Downstate capacitance simulated using FEM tool.

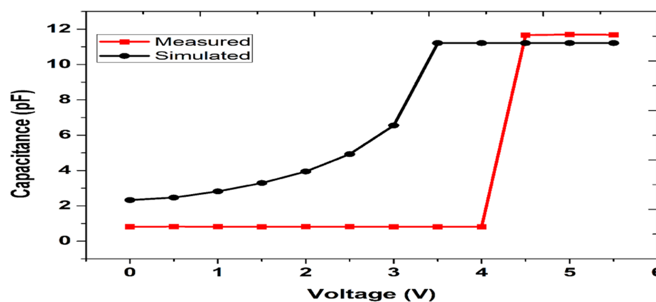

FIGURE 16. C–V characteristics of proposed switch (simulated & measured).

the switch under various voltage conditions and validate its functionality.

To further validate the experimental results, the measured displacement values can be compared with simulated values obtained using finite element method (FEM) tools. FEM simulations enable the prediction of the expected displacement based on the applied voltages and the structural properties of the switch. By comparing the experimental and simulated values, researchers can evaluate the accuracy of the simulations and gain a deeper understanding of the switch's behavior. The close approximation between the measured and simulated displacement values indicates the reliability and accuracy of the FEM model in predicting the switch's response. This agreement strengthens the confidence in the design and performance of the RF MEMS switch and supports its suitability for use in RF applications.

The observed pull-in voltage of the proposed switch is measured to be 4.4 V, while the simulated value is 4.01 V Fig.13. The deviation between the measured and simulated values can be attributed to factors such as air damping and dimensional tolerances in the structure. These factors can introduce variations in the switch's behavior and affect its electrical characteristics. The applied voltage difference between the switch membrane and the biasing pads plays a crucial role in the switch's operation. This voltage difference causes the membrane to move closer to the signal line, reducing the air gap between them. As a result, the parallel plate capacitance between the membrane (acting as the top plate) and the biasing pads and signal line (acting as the bottom plate) increases.

The upstate capacitance refers to the capacitance developed between the membrane and the signal line when a voltage of 1 mV is applied to the signal line without any voltage supplied to the biasing pads. This capacitance can be simulated and observed, as shown in Fig. 14.

When a DC voltage is applied to the biasing pads, an additional capacitance is developed between the membrane and the biasing pads. This increases the overall capacitance by expanding the capacitive area and the distance between the membrane and the bottom plates. This capacitance is referred to as the downstate capacitance, and its simulation result is presented in Fig. 15. To calibrate the capacitance for different voltages, measurements are performed using the DC probe station. The calibration process involves applying various voltages and measuring the corresponding capacitance values. The results of the capacitance calibration are depicted in Fig. 16, and the extracted capacitance values are obtained for different voltage levels. By calibrating the capacitance values for different voltages, researchers can understand and characterize the switch's electrical behavior, providing valuable insights for its optimization and performance evaluation.

TABLE 2. Capacitance Values of Proposed Switch at Up and Downstate Conditions

Component	Analytical	Simulated	Measured
Upstate	74.2 fF	85.3 fF	81.2 fF
Downstate	11.27 pF	11.212 pF	11.61 pF

pF: picofarads; fF: Femtofarads

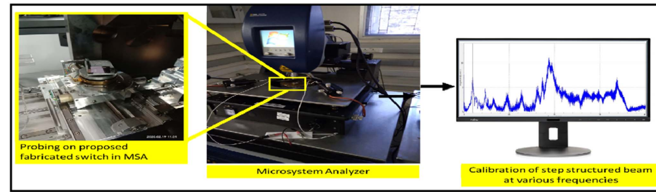

FIGURE 17. Experimental set up of lase Doppler vibrometer.

From the Fig. 16, it is observed that the switch shows the rapid increase in the capacitance from 0.81 pF to 11.6 pF from upstate to downstate condition. The analytical, simulated and measured capacitance values are presented in the Table 2 to observe the close approximation of values for validation.

B. MECHANICAL CHARACTERISTICS

The microsystem analyzer, also known as a Laser Doppler vibrometer (LDV), is a device used to measure the mechanical resonant frequency of a suspended membrane in a proposed switch. The LDV utilizes the principles of laser Doppler velocimetry to analyze the motion of the membrane. In the experimental setup shown in Fig. 17, the LDV is employed to perform the frequency testing. The LDV consists of a laser beam source that emits a coherent laser beam onto the surface of the suspended membrane. The laser beam reflects off the membrane surface and is collected by a detector. As the membrane vibrates due to the applied stimulus or external forces, the reflected laser beam undergoes a frequency shift known as the Doppler shift. This shift is directly proportional to the velocity of the membrane's motion. The LDV's detector measures this Doppler shift and provides information about the membrane's vibration characteristics. By analyzing the Doppler shift, the LDV can determine the mechanical resonant frequency of the suspended membrane. The resonant frequency corresponds to the frequency at which the membrane vibrates most efficiently or with the highest amplitude. It's worth noting that the LDV mentioned in the description has a frequency testing capability up to 1 MHz. This means that the device can accurately measure the mechanical resonant frequency of the suspended membrane within the range of 0 Hz to 1 MHz.

An input inline pressure of 0.1 MPa is applied on the switch membrane and made to vibrate up and down. The membrane displaces maximum of 2 μm at its natural frequency and it is noted as shown in the Fig. 18.

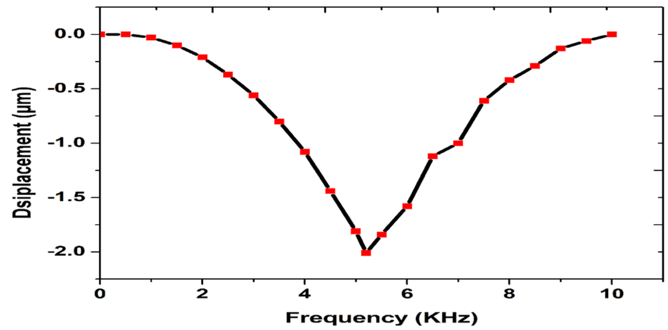

FIGURE 18. Frequency analysis of proposed switch.

TABLE 3. Comparison of Various Components of the Proposed Switch at Up and Downstate Conditions

Component	Simulated	Measured
Resonant Frequency	4.185 KHz	4.6 KHz
Quality Factor	0.02	0.031
Switching time	99 μsec	93 μsec

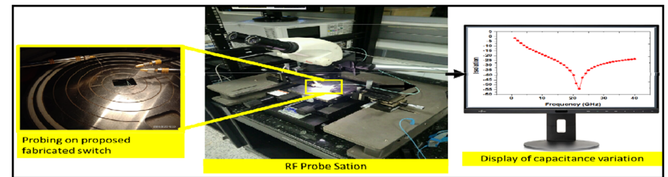

FIGURE 19. Proposed switch loaded on RF probe station.

The switch membrane is calibrated to vibrate at different frequencies. The switch displaces maximum of 2 μm at the frequency of 4.6 KHz, other than that frequency the membrane displaces less than 2 μm. the uniformity in the displacement is observed below the resonant frequency and non – uniformity in the displacement occurs due to mechanical stiffness of the membrane which opposes the input pressure. The quality factor and time taken to switch the membrane from upstate to down state are extracted with the microsystem analyser and obtained as 0.031 and 93 μsec respectively. The simulated and measured values are presented and compared in the Table 3.

C. RF CHARACTERISTICS

The Vector Network Analyzer (RF Probe Station) is used to measure the electromagnetic properties of proposed RF MEMS Switch. The wafer is sliced into a small piece which contains the proposed switches. Initially calibration of the RF probe station is done for a half an hour between the frequencies of 1 GHz to 40 GHz [23]. After the calibration, these wafers are loaded on the RF Probe Station as shown in the Fig. 19. The RF probe station contains three terminals, an input power terminal which is feed to the signal line of

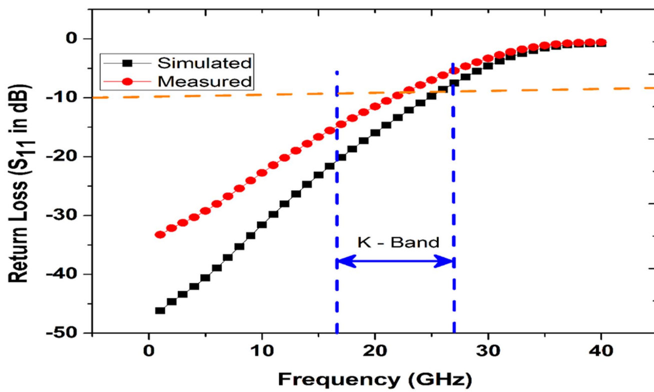

FIGURE 20. Return losses of proposed switch.

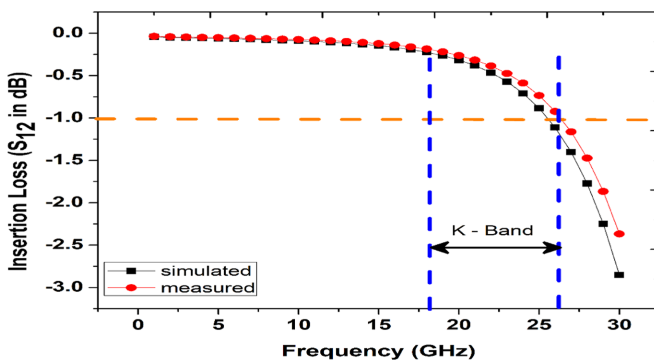

FIGURE 21. Insertion losses of fabricated switch.

the CPW, a ground terminal connected to the ground lines of CPW and an input voltage terminal which is used to supply the biasing voltage to the biasing pads. Initially, when no voltage is supplied by the third terminal, the membrane is not actuated and power of 1W is feed to the signal line. The return and insertion losses are measured during this stage and are presented in the Figs. 20 and 21 respectively. The results are extracted from the RF probe station.

Fig. 21, it is evident that the proposed switch design exhibits good return loss characteristics. Return loss is a measure of the reflected power at a specific frequency, and lower return loss values indicate better impedance matching and reduced power loss. The fabricated switch demonstrates a return loss of less than −10 dB up to a frequency of 25 GHz, while the simulated switch achieves this up to 26 GHz. This suggests that both the fabricated and simulated switches have good impedance matching and low power reflection within the respective frequency ranges. Specifically, at 18 GHz, the experimental return loss of the switch is reported as −13.4 dB. In comparison, the corresponding simulated value is −18.6 dB. This indicates a reasonably close agreement between the experimental and simulated results, with the simulated value showing a slightly better return loss. Similarly, at 26 GHz, the experimental return loss of the switch is −10.64 dB, while the simulated return loss is −12.59 dB. Again, there is a

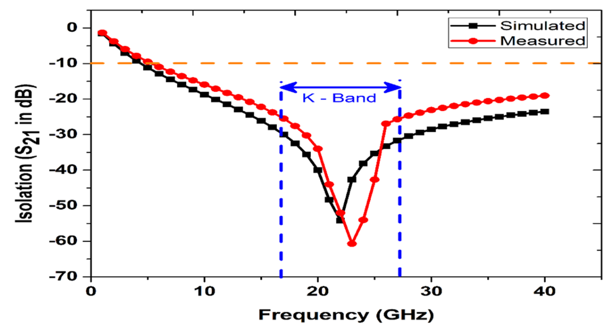

FIGURE 22. Isolation of fabricated switch.

relatively good agreement between the experimental and simulated values, indicating effective impedance matching and reduced power reflection at this frequency.

From Fig. 22, it is evident that the fabricated switch exhibits very low insertion loss, which refers to the amount of signal power lost when passing through the switch. The low insertion loss is attributed to the low upstate capacitance developed by the step-down structured beam. Specifically, at 18 GHz, the switch demonstrates an insertion loss of −0.186 dB, indicating efficient signal transmission. At 26 GHz, the insertion loss is slightly higher at −0.9 dB, still within acceptable limits for the targeted frequency range. The switch is designed to operate within the frequencies of the K-band, which typically span from 18 GHz to 26 GHz. By optimizing the dimensions and materials used in the fabrication process, the switch has achieved favorable results, demonstrating its suitability for K-band applications.

The switch is supplied with a biasing voltage that is equal to the pull-in voltage of the switch. The isolation (S21) of the switch is then measured using an RF probe station. The switch undergoes testing over a frequency range of 1 GHz to 40 GHz to determine its resonant frequency. The resonant frequency refers to the frequency at which the switch exhibits optimal performance characteristics. During the actuation of the switch's membrane, it successfully isolates the input and output terminals of the CPW (coplanar waveguide). This state of actuation is referred to as the "OFF" state of the switch, where no signal passes through the CPW. This OFF state demonstrates the switch's ability to effectively block signal transmission. At a frequency of 23 GHz, which corresponds to the resonant frequency of the transmission signal, the switch achieves excellent isolation of −60.1 dB. This indicates a significant reduction in the leakage of signals between the input and output terminals. Furthermore, the switch maintains isolation of less than −10 dB across a wide frequency range from 10 GHz to 60 GHz, demonstrating its efficient operation within the K-band frequencies. To compare the simulated and measured performance of the switch, S-parameters (scattering parameters) are presented in Table 4. S-parameters provide information about the behavior of a linear electrical network, including transmission and reflection characteristics. The comparison between simulated

TABLE 4. S–Parameters of Proposed Switch at Resonant Frequency 23 GHz

Component	Simulated	Measured
Return Loss	-12.10335	-10.53
Insertion Loss	-0.57164	-0.47446
Isolation	-42.65788	-60.68023

FIGURE 23. Proposed antenna structure (a) patch A (b) patch B.

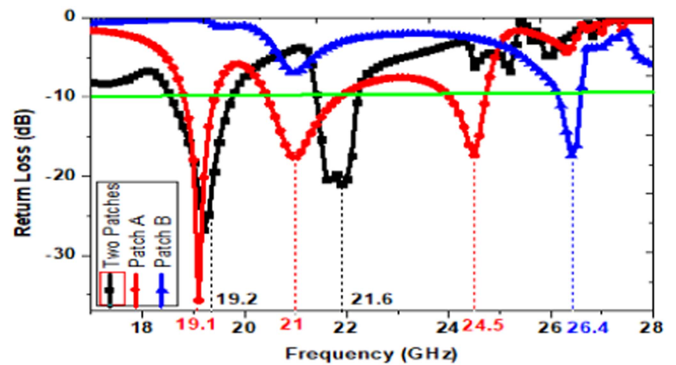

FIGURE 24. Return losses of proposed antenna operated by integrated switches.

and measured S-parameters allows for the validation of the switch's performance against the expected values.

D. ANTENNA INTEGRATED WITH THE PROPOSED RF EMS SWITCH

The integration of the patches is achieved through a step structured RF MEMS switch. Fig. 23(a) and (b) likely illustrate the physical layout or schematic representation of the antenna and its components. Patch A has a radius of 2680 µm, while Patch B has a radius of 2000 µm. Both patches are specifically designed to radiate signals within the K-band frequencies, which typically range from 18 GHz to 27 GHz. To enable the selective radiation of signals through the patches, the proposed design incorporates two RF MEMS switches. These switches are positioned 500 µm away from the patches, providing isolation during switch actuation. Switch A is placed over the feed line of Patch A, while Switch B is positioned over the feed line of Patch B. The alternating actuation of the switches allows for the transmission of signals through the respective patches. By controlling the states of the switches, the antenna can switch between using Patch A or Patch B for signal radiation, providing flexibility and reconfigurability in the antenna's operation. Overall, the described antenna design employs RF MEMS switches to enable the selective radiation of signals through Patch A and Patch B. The switches are strategically positioned to isolate the patches during actuation, ensuring proper functionality of the antenna.

E. RETURN LOSS OF ANTENNA

Initially, when neither switch is actuated and the DC biasing voltage is applied, the antenna operates in an "upstate." In this state, the step structured beam is formed, allowing the signal to pass into both patches and radiate the RF signal. Both patches are in a radiating mode, and the total length of the radiating patch is the sum of the lengths of the two patches. When switch B is actuated, and switch A remains unactuated (OFF condition), the signal is transmitted into patch A, which has a radius of 2680 µm. This configuration causes the antenna to primarily radiate through patch A. Conversely, when switch A is actuated, and switch B remains unactuated, switch B is in the ON state, allowing the signal to radiate through patch B while switch A is in the OFF condition. Patch B has a radius of 2000 µm, and in this configuration, the antenna predominantly radiates using patch B. The return losses obtained during these different configurations are depicted in Fig. 24. Return loss is a measure of the amount of reflected power at a specific frequency. It provides insights into the efficiency of signal transmission and the matching of impedance between the antenna and the transmission line. By studying the return losses, one can assess the antenna's performance and the effectiveness of the different patch configurations in transmitting the RF signal.

During the ON state of both switches, the antenna radiates the signal using both patches. The first resonance frequency is observed at 19.2 GHz, with a return loss of −26.7 dB, indicating efficient signal transmission and minimal reflected power. The antenna also exhibits a second resonance frequency at 21.6 GHz, with a return loss of −20.4 dB. Switch B is then actuated, enabling the OFF condition, and only patch A radiates the signal. At the first resonance frequency of 19.1 GHz, the return loss is −35.6 dB, indicating even better signal transmission efficiency. Additionally, the antenna demonstrates second and third resonant frequencies at 21 GHz and 24.5 GHz, with return losses of −17.6 dB and −17.3 dB, respectively. When switch A is actuated, patch A is disconnected, and only patch B radiates the signal at 26.4 GHz, with a return loss of −17.47 dB. However, when both switches are actuated, both patches are disconnected from the feed line, resulting in no signal radiation from either patch. In summary, the proposed antenna design exhibits reconfigurability at different frequencies in the K-band by alternating the RF MEMS switches. The return loss values indicate the efficiency of signal transmission, and the resonance frequencies demonstrate the antenna's ability to operate at multiple frequencies, making it suitable for dual-frequency applications.

F. GAIN AND RADIATION CHARACTERISTICS OF ANTENNA

The passage emphasizes the importance of gain and radiation patterns in antenna characteristics for evaluating signal

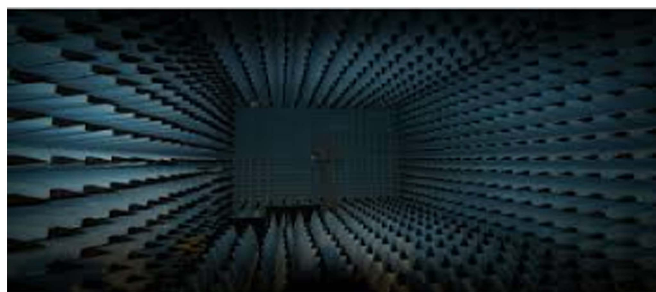

FIGURE 25. Anechoic chamber to measure the radiation pattern.

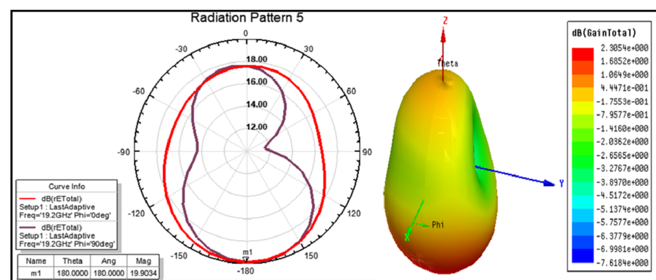

FIGURE 26. Radiation pattern during both the switches are in ON condition.

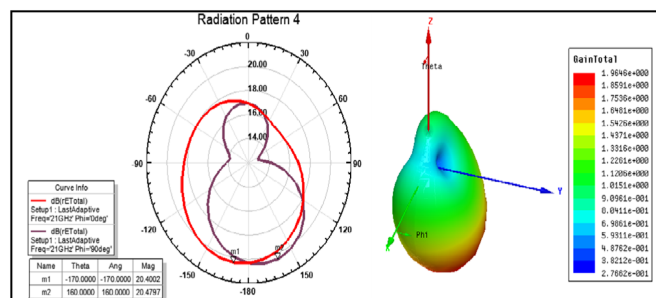

FIGURE 27. Radiation pattern switch A in ON condition.

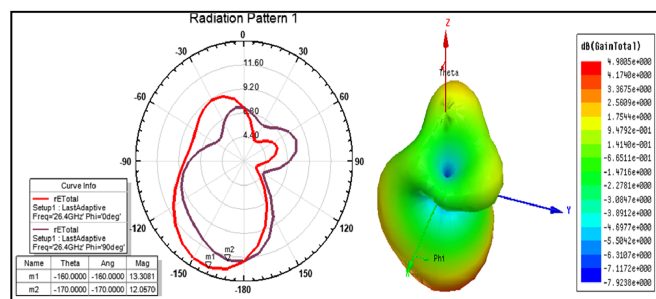

FIGURE 28. Radiation pattern switch B in ON condition.

strength and the direction of signal propagation. These characteristics are typically studied in an anechoic chamber, as depicted in Fig. 25. An anechoic chamber is a specialized room designed to minimize reflections of electromagnetic waves, creating an environment that approximates free space conditions. It typically features radiation-absorbing materials on the walls, ceiling, and floor to reduce reflections and external interference. By conducting measurements in an anechoic chamber, researchers can obtain accurate and reliable data on the gain and radiation patterns of an antenna. The gain of an antenna refers to its ability to direct and concentrate transmitted or received power in a particular direction. It is often expressed in decibels (dB) and indicates the strength of the signal in the intended direction compared to a reference antenna. Radiation patterns describe how an antenna distributes power in different directions in three-dimensional space. They provide valuable information about the antenna's directional properties, beamwidth, and side lobes. Radiation patterns are typically represented as graphs or diagrams showing signal strength as a function of angle. By studying gain and radiation patterns in an anechoic chamber, researchers can assess the performance and suitability of an antenna for specific applications. These measurements help ensure optimal signal transmission and reception by understanding how the antenna radiates energy and in which directions it has the strongest and weakest signals.

The passage describes the radiation pattern characteristics of a proposed antenna design. The radiation patterns of both the electric field ($\Phi = 0°$) and magnetic field ($\Phi = 90°$) are observed at different θ values. Several figures are referenced to illustrate the antenna's performance under different conditions. In Fig. 26, during the ON condition of both switches, the antenna demonstrates an electric field and a magnetic field of 19.9 dB at a frequency of 19.2 GHz. The maximum gain of 1.7 dB is observed at an angle of 180°. Fig. 27 depicts the scenario where only patch A radiates the signal by activating switch B. In this case, the antenna exhibits an electric field intensity of 20.4 dB at an angle of $-170°$ and a magnetic field of 20.47 dB at an angle of 180°. The gain reaches 1.96 dB. Fig. 28 represents the situation where only patch B radiates the signal by enabling switch A in the OFF condition. The antenna produces an electric field distribution of 13.3 dB at an angle of $-160°$ and a magnetic field of 12.06 dB at an angle of $-170°$. The gain achieved is 1.98 dB. Overall, the proposed antenna design demonstrates the ability to reconfigure polarization through the utilization of RF MEMS switches. These switches effectively enable the antenna to adapt for K-band applications.

V. CONCLUSION

The article presents a novel approach to fabricating a step structure switch integrated on a circular patch antenna using surface micromachining technology. The dimensions of both the switch and antenna are optimized to ensure transmission of RF signals within the K-band frequency range. The switch is designed to operate at a low pull-in voltage of 4.4 V, indicating its energy efficiency. Additionally, it exhibits a low on-state capacitance of 81.2 fF, which suggests reduced power consumption and improved performance. At the frequency of

23 GHz, which is the central frequency of the K-band, the switch demonstrates high isolation of −60.68 dB. This high isolation indicates efficient blocking of signals and minimal leakage between the input and output terminals. By integrating the switch with the circular patch antenna, the antenna gains reconfigurability in its operating frequency. When both switches are in the on-state, the antenna radiates the signal at a frequency of 19.2 GHz with a return loss of −26.7 dB. This indicates efficient signal transmission and impedance matching at that frequency. When only switch A is in the on-state, the antenna radiates at 21 GHz with a return loss of −17.6 dB. Similarly, when only switch B is in the on-state, the antenna radiates the signal at 26.4 GHz with a return loss of −17.47 dB. These results demonstrate the successful frequency reconfiguration capability achieved by incorporating the step structured RF MEMS switches.

The proposed antenna, integrated with the switches, holds potential for various K-band applications, including surface movement radars, direct broadcast satellite systems, DHT (Digital High-definition Television), and 5G mobile communication. These applications can benefit from the reconfigurability and optimized performance of the proposed antenna design. Overall, the article highlights the successful integration of the step structure switch with the circular patch antenna, leading to reconfigurable frequency operation within the K-band range. The proposed design holds promise for various K-band applications, leveraging the advantages of RF MEMS switches in enhancing antenna performance

REFERENCES

[1] R. E. Mihailovich et al., “MEM relay for reconfigurable RF circuits,” *IEEE Microw. Wireless Compon. Lett.*, vol. 11, no. 2, pp. 53–55, Feb. 2001.

[2] D. Hyman et al., “Surface-micromachined RF MEMS switches on GaAs substrates,” *Int. J. RF Microw. Comput.-Aided Eng.*, vol. 9, pp. 348–361, Aug. 1999.

[3] S. Duffy et al., “MEMS microswitches for reconfigurable microwave circuitry,” *IEEE Microw. Wireless Compon. Lett.*, vol. 11, no. 3, pp. 106–108, Mar. 2001.

[4] K. G. Sravani, K. Guha, and K. S. Rao, “Design of a novel step structure RF MEMS switch for K-band applications,” *Microsystem Technol.*, vol. 27, pp. 619–627, Jul. 2020.

[5] P. M. Zavracky, N. E. M. Gruer, R. H. Morrison, and D. Potter, “Microswitches and microrelays with a view toward microwave applications,” *Int. J. RF Microw. Comput.-Aided Eng.*, vol. 9, pp. 338–347, Jul. 1999.

[6] C. L. Goldsmith, Z. Yao, S. Eshelman, and D. Denniston, “Performance of low-loss RF MEMS capacitive switches,” *IEEE Microw. Guided Wave Lett.*, vol. 8, no. 8, pp. 269–271, Aug. 1998.

[7] K. G. Sravani, K. Guha, and K. S. Rao, “An analytical capacitance modeling of step structured perforated RF MEMS switch,” *Microsystem Technol.*, vol. 28, pp. 771–778, Aug. 2022.

[8] G. L. Tan and G. M. Rebeiz, “DC-26 GHz MEMS series-shunt absorptive switches,” in *Proc. IEEE MTT-S Int. Microw. Symp. Dig.*, 2001, pp. 325–328.

[9] D. Peroulis, K. Sarabandi, and L. P. B. Katehi, “Low contact resistance series MEMS switches,” in *Proc. IEEE MTT-S Int. Microw. Symp. Dig.*, 2002, pp. 223–226.

[10] K. G. Sravani, K. Guha, and A. Elsinawi, “Design and optimisation of a novel structure capacitive RF MEMS switch to integrate with an antenna to improve its performance parameters,” *Inst. Eng. Technol. Circuits, Devices Syst.*, vol. 14, no. 3, pp. 276–287, Nov. 2019.

[11] K. G. Sravani, K. Guha, K. S. Rao, and A. Elsinawi, “Design of a novel structure capacitive RF MEMS switch to improve performance parameters,” *Inst. Eng. Technol. Circuits, Devices Syst.*, vol. 13, no. 7, pp. 1093–1101, Jul. 2019.

[12] J. B. Muldavin and G. M. Rebeiz, “High-isolation CPW MEMS shunt switches—Part 1: Modeling,” *IEEE Trans. Microw. Theory Tech.*, vol. 48, no. 6, pp. 1045–1052, Jun. 2000.

[13] K. G. Sravani, K. Guha, and K. S. Rao, “A modified proposed capacitance model for step structure capacitive RF MEMS switch by incorporating fringing field effects,” *Int. J. Electron.*, vol. 107, pp. 1822–1843, May 2020.

[14] G. M. Rebeiz and J. B. Muldavin, “RF MEMS switches and switch circuits,” *IEEE Microw. Mag.*, vol. 2, no. 4, pp. 59–71, Dec. 2001.

[15] S. P. Pacheco, L. P. B. Katehi, and C. T.-C. Nguyen, “Design of low actuation voltage RF MEMS switch,” in *Proc. IEEE MTT-S Int. Microw. Symp. Dig.*, 2000, pp. 165–168.

[16] D. Peroulis, S. Pacheco, K. Sarabandi, and P. B. Katehi, “MEMS switches for high-isolation switching and tunable filtering,” in *Proc. IEEE MTT-S Int. Microw. Symp. Dig.*, 2000, pp. 1217–1220.

[17] K. G. Sravani, K. Guha, and K. S. Rao, “Analysis of a novel RF MEMS switch using different meander techniques,” *Microsystem Technol.*, vol. 26, no. 5, pp. 1625–1635, 2020.

[18] N. S. Barker and G. M. Rebeiz, “Optimization of distributed MEMS transmission-line phase shifters—U-band and W-band design,” *IEEE Trans. Microw. Theory Tech.*, vol. 48, no. 11, pp. 1957–1966, Nov. 2000.

[19] K. S. Rao, L. N. Thalluri, K. Guha, and K. G. Sravani, “Fabrication and characterization of capacitive RF MEMS perforated switch,” *IEEE Access*, vol. 6, pp. 77519–77528, 2018.

[20] M. Angira and K. Rangra, “A novel design for low insertion loss, multi-band RF-MEMS switch with low pull-in voltage,” *Eng. Sci. Technol., Int. J.*, vol. 19, no. 1, pp. 171–177, 2016.

[21] K. S. Rao et al., “Design and simulation of fixed–fixed flexure type RF MEMS switch for reconfigurable antenna,” *Microsystem Technol.*, vol. 27, pp. 455–462, 2018.

[22] A. K. Ravirala et al., “Design and performance analysis of uniform meander structured RF MEMS capacitive shunt switch along with perforations,” *Microsystem Technol.*, vol. 24, no. 2, pp. 901–908, Feb. 2018, doi: 10.1007/s00542-017-3403-z.

[23] J. S. Hayden and G. M. Rebeiz, “Low-loss cascadable MEMS distributed X-band phase shifters,” *IEEE Microw. Guided Wave Lett.*, vol. 10, no. 4, pp. 142–144, Apr. 2000.